Astronomy & Astrophysics

StarHorse results for spectroscopic surveys with *Gaia* EDR3: Chrono-chemical populations in the solar vicinity, the genuine thick disk, and young alpha-rich stars[*]
(Corrigendum)

A. B. A. Queiroz[1,2,3], F. Anders[4,5,6], C. Chiappini[1,3], A. Khalatyan[1], B. X. Santiago[7,3], S. Nepal[1,2],
M. Steinmetz[1], C. Gallart[8,9], M. Valentini[1], M. Dal Ponte[7,3], B. Barbuy[10], A. Pérez-Villegas[11],
T. Masseron[8,9], J. G. Fernández-Trincado[12], S. Khoperskov[1], I. Minchev[1], E. Fernández-Alvar[8,9],
R. R. Lane[13], and C. Nitschelm[14]

[1] Leibniz-Institut für Astrophysik Potsdam (AIP), An der Sternwarte 16, 14482 Potsdam, Germany
    e-mail: aqueiroz@aip.de
[2] Institut für Physik und Astronomie, Universität Potsdam, Haus 28 Karl-Liebknecht-Str. 24/25, 14476 Golm, Germany
[3] Laboratório Interinstitucional de e-Astronomia – LIneA, Rua Gal. José Cristino 77, Rio de Janeiro, RJ 20921-400, Brazil
[4] Dept. de Física Quàntica i Astrofísica (FQA), Universitat de Barcelona (UB), C. Martí i Franqués, 1, 08028 Barcelona, Spain
[5] Institut de Ciències del Cosmos (ICCUB), Universitat de Barcelona (UB), C. Martí i Franqués, 1, 08028 Barcelona, Spain
[6] Institut d'Estudis Espacials de Catalunya (IEEC), C. Gran Capità, 2-4, 08034 Barcelona, Spain
[7] Instituto de Física, Universidade Federal do Rio Grande do Sul, Caixa Postal 15051, Porto Alegre, RS 91501-970, Brazil
[8] Instituto de Astrofísica de Canarias, 38205 La Laguna, Tenerife, Spain
[9] Departamento de Astrofísica, Universidad de La Laguna, 38200 La Laguna, Tenerife, Spain
[10] Department of Astronomy, Universidade de São Paulo, São Paulo 05508-090, Brazil
[11] Instituto de Astronomía, Universidad Nacional Autónoma de México, A.P. 106, 22800 Ensenada, B. C., Mexico
[12] Instituto de Astronomía, Universidad Católica del Norte, Av. Angamos 0610, Antofagasta, Chile
[13] Centro de Investigación en Astronomía, Universidad Bernardo O'Higgins, Avenida Viel 1497, Santiago, Chile
[14] Centro de Astronomía, Universidad de Antofagasta, Avenida Angamos 601, Antofagasta 1270300, Chile

1. Introduction

We have identified an unintentional age prior used for the StarHorse calculations presented in this paper. Instead of using a broad Gaussian age prior for the thin disk population as in Queiroz et al. (2018), we inadvertently used a prior based on the star formation history of Mor et al. (2018). This prior had an impact on the derived masses and ages of sub-giant and main-sequence turn-off stars of the thin disk, affecting mainly the oldest ages. To address this issue, we have corrected the problem in our code and replaced the affected files; the replacements are now referred to as v2. It is important to note that the distances, extinctions, surface gravity, and temperatures provided by StarHorse were not affected by this problem. In this erratum, we present updated table numbers and figures reflecting the corrected ages. It is important to emphasise, however, that the scientific conclusions drawn from our original analysis remain unchanged, with the primary change being a slightly (4%) older age for the genuine thick disk compared to previously reported values.

Table 1. Mean and standard deviation of each age prior.

Component	μ	σ
Thin disk	5.0 Gyr	4 Gyr
Thick disk	10.5 Gyr	2 Gyr
Bulge	10.0 Gyr	3 Gyr
Halo	12.5 Gyr	1 Gyr

2. Age prior of the thin disc

StarHorse uses age and metallicity priors for the main galactic components: thin and thick disks, bulge, and halo (for details see Queiroz et al. 2018). The thin-disk prior, $P_{\text{thin}}(\tau_0)$, was inadvertently set to use a piece-wise star formation history, inspired by the work of Mor et al. (2018):

$$P_{\text{thin}}(\tau_0) = \left\{ \begin{array}{ll} \frac{1}{10 \cdot (e-1)} \cdot e^{0.1\tau_0} & \text{if } \tau_0 \leq 10 \\ 0 & \text{else} \end{array} \right\}, \tag{1}$$

where τ_0 is the age of a particular stellar model.

We have now reset the age priors to be consistent with our description in previous papers (Queiroz et al. 2018, 2020, 2023). We note that the use of the piece-wise prior for the thin disk
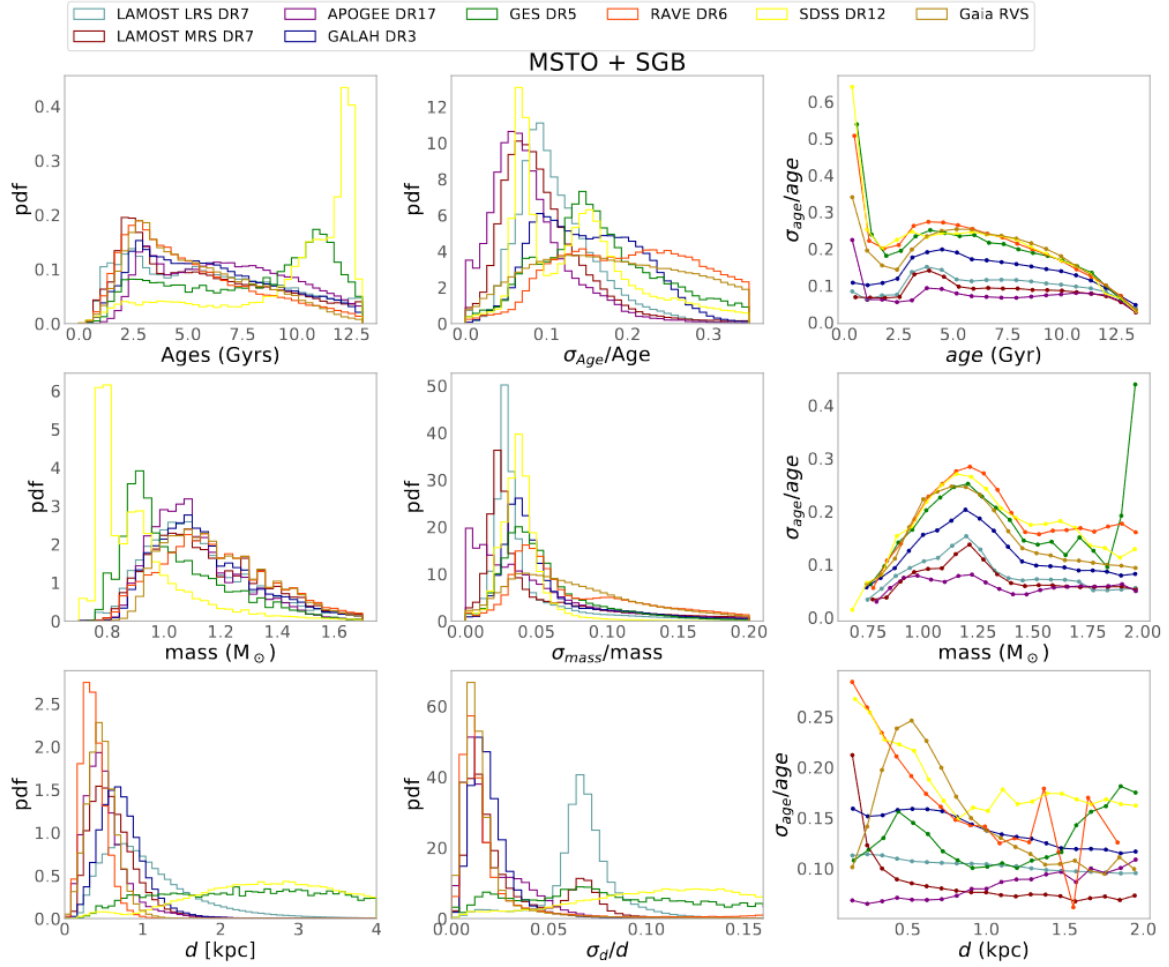
Fig. 1. Distributions of ages, masses, distances, and their uncertainties for the MSTO+SGB samples. The *y*-axis shows the probability density. All histograms are normalised so that the area under the histogram integrates to 1. The right panels show the mean age uncertainty per bin of age, mass, and distance for each survey.

Table 2. Mean relative error or uncertainty per `StarHorse` output parameter per spectroscopic survey.

Survey	$\sigma_{\rm d}/d$ (%)	σ_{A_V} (mag)	$\sigma_{T_{\rm eff}}/T_{\rm eff}$ (%)	$\sigma_{\rm [M/H]}$ (dex)	$\sigma_{\log g}$ (dex)	σ_{m_*}/m_* (%)	$\sigma_{\rm age}/{\rm age}_{\rm MSTO+SGB}$ (%)	$\sigma_{\rm age}/{\rm age}_{\rm SGB}$ (%)
LAMOST DR7 LRS	7.5	0.082	0.8	0.067	0.053	4.53	11.3	16.6
LAMOST DR7 MRS	4.9	0.129	0.9	0.072	0.042	6.2	10.4	9.37
SDSS DR12 optical	10	0.075	1.6	0.093	0.080	4.01	15.21	11.1
GALAH+ DR3	3.6	0.092	1.3	0.092	0.041	5.89	15.5	9.79
RAVE DR6	5.1	0.099	1.6	0.099	0.058	8.82	23.4	19.30
APOGEE DR17	4.3	0.178	0.4	0.029	0.021	6.28	8.11	6.57
GES DR5	5.8	0.099	1.2	0.076	0.053	5.94	18.5	18.87
Gaia DR3 RVS	3.1	0.069	1.3	0.172	0.044	8.98	21.5	12.2

produced a sharp cut at the oldest thin disk ages. In all catalogues available at AIP[1] and at the CDS, the age and mass values have been replaced by the results from the calculation that used the prior given in Eq. (2) with mean, μ, and standard deviation, σ, specified in Table 1, also described in Queiroz et al. (2018). The results have been replaced for the Main Sequence Turnoff (MSTO) and Subgiant Branch (SGB) phases of stellar evolution

for which `StarHorse` ages are available.

$$P(\tau_0) = \frac{1}{\sigma\sqrt{2\pi}} \exp\left(-\frac{1}{2}\frac{(\tau_0 - \mu)^2}{\sigma^2}\right). \tag{2}$$

In the following sections we show the updated figures and tables from Queiroz et al. (2023, hereafter Q23) that were affected by the described error. We only reproduce the figures that show significant differences, nothing that the prior in Eq. (1) mainly affected old stars (≥9 Gyr).
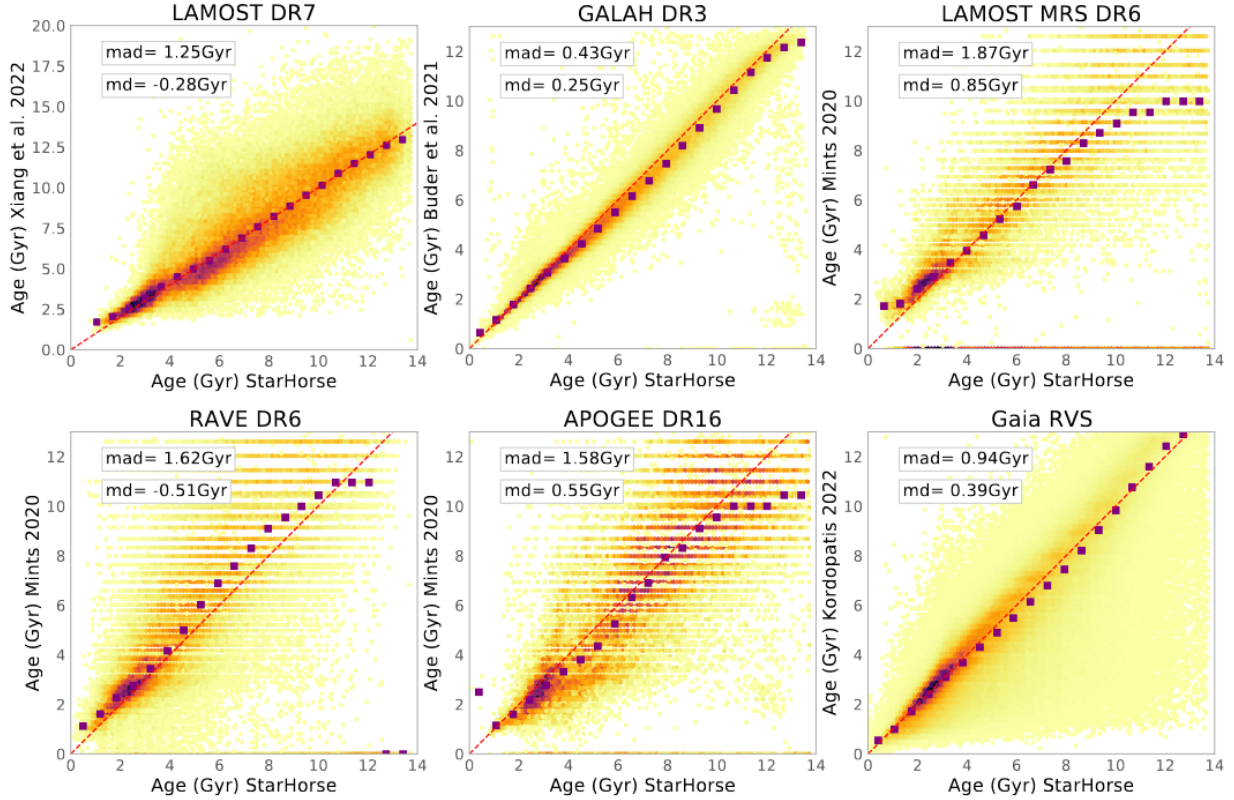
---

[1]   data.aip.de

Fig. 2. Comparison of our MSTO+SGB age estimates with values from the recent literature.

Table 3. Configuration and input parameters of t-SNE+HDBSCAN.

t-SNE configuration			
Survey	Input	Perplexity	Random state
APOGEE DR17	$[(Mg, Mn, Al, Si)/Fe] + Age_{SH}$	80	50
GALAH DR3	$[(Mg, Al, Si, Ni, Zn, Y, Ba)/Fe] + Age_{SH}$	100	50
LAMOST DR7	$[(C, Mg, Si)/Fe] + Age_{SH}$	45	150
HDBSCAN configuration			
Survey	min_cluster_size	min_samples	cluster_selection_epsilon
APOGEE DR17	38	1	0.6
GALAH DR3	45	15	1.7
LAMOST DR7	207	8	1.95

3. Impact on figures and tables in the article

Figure 6 in Q23 (here Fig. 1) showed a strong discontinuity towards old ages (especially for surveys for which the uncertainties in the stellar parameters were larger, as expected). The new Fig. 1 shows a smoother transition between young and old stars, accompanied by a more realistic and broader distribution of uncertainties. In Table 2, we have updated the mean uncertainty values for ages and masses. However, here the changes in age have been minor, as expected given that mostly the oldest stars were affected. The mass distribution remains largely unchanged from the previous run of StarHorse.

Regarding the validation of young ages through the comparison with ?, our results remain consistent. However, when comparing with other isochrone ages, we observe significant improvements, particularly for stars older than 10 Gyr. This improvement is prominently reflected in our updated Fig. 2 (cf. Fig. 9 in Q23). Especially for the *Gaia* Data Release (DR) 3

Radial Velocity Spectrometer (RVS) data, there is now a much better agreement with the work of Kordopatis et al. (2023).

We conducted an extensive review of our findings from Sect. 5 of Q23 and find that the majority of our results remain mostly unchanged, including the slope of the chemical clocks. Furthermore, Fig. 3, which depicts the distribution of alpha abundances versus age is improved. It is worth noting that a reduction in the age spread is observable in the high-alpha population, which is typically associated with an older population (see e.g. Miglio et al. 2021).

4. Impact on the t-SNE age-abundance analysis

In our analysis we used elemental abundances and ages as inputs to the t-distributed stochastic neighbor embedding (t-SNE). Therefore, in this section we redo the full analysis and summarise how the results were affected.
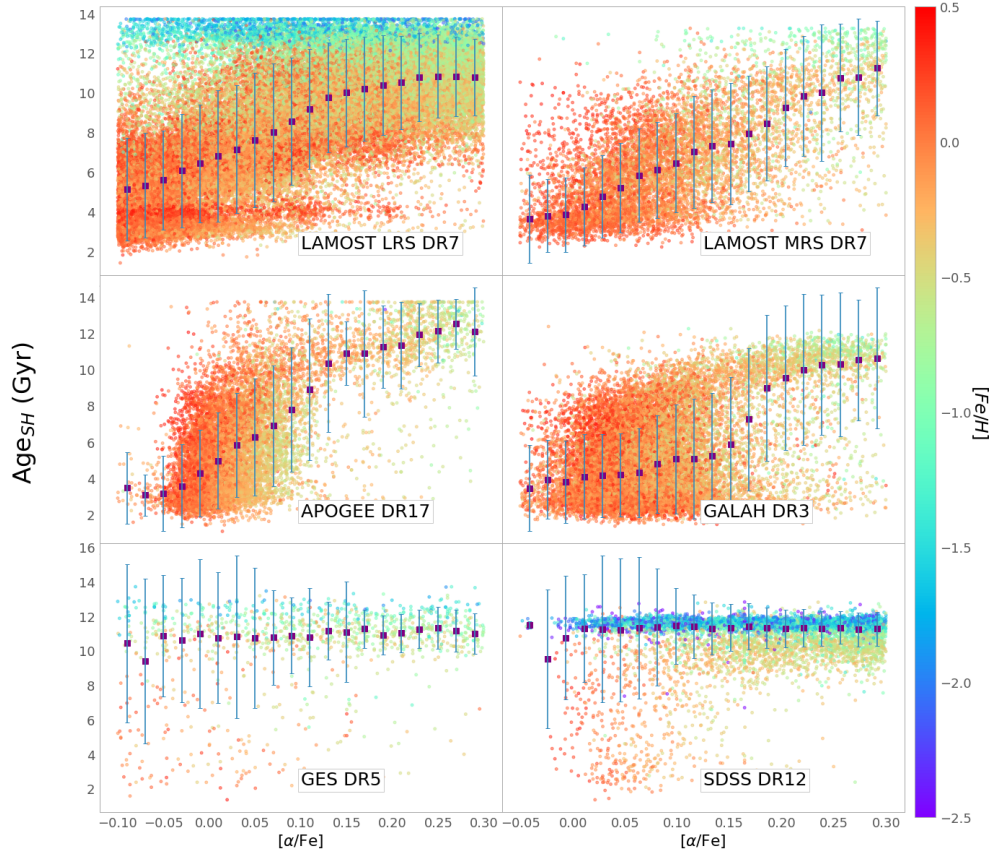
Fig. 3. [α/Fe] versus age distribution for the MSTO+SGB samples of each survey. A cleaning per signal to noise and suggested flags was performed. The purple squares show the median trend per bin in [α/Fe], while the error bars show its one σ deviation. We only display the surveys that have mean statistical uncertainty in age < 20% according to Table 2 (no RAVE or *Gaia* RVS). We also performed a cleaning of flags in the [α/Fe] determination from each survey.
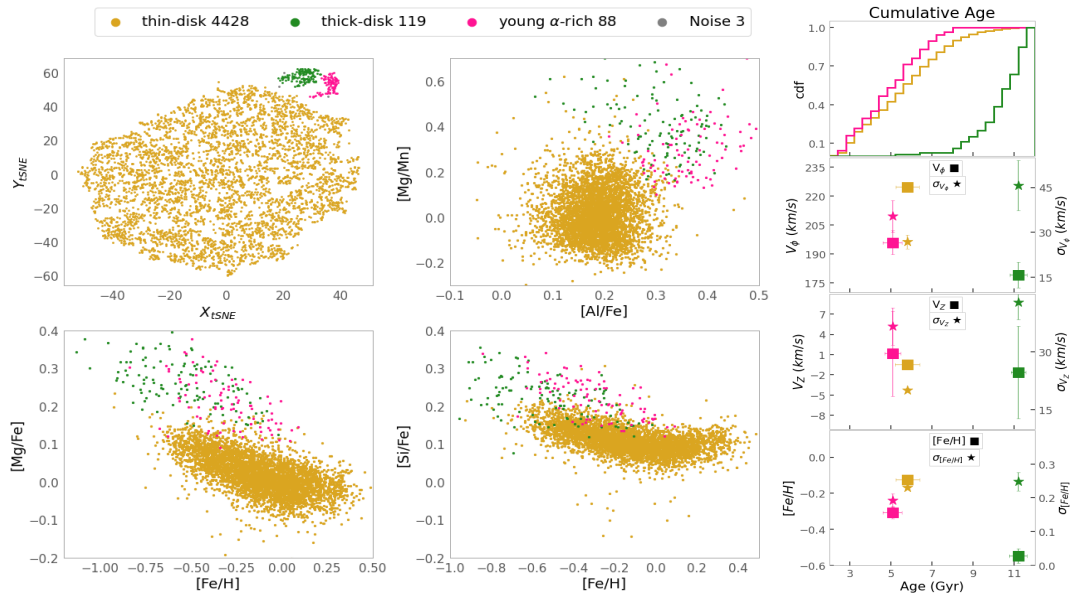

Fig. 4. General results of the t-SNE+HDBSCAN application. Upper-left panel: t-SNE projection for SGB stars in APOGEE DR17. Colours correspond to different groups found by t-SNE+HDBSCAN on the data. Lower-left and middle panels: abundance ratios of α elements to those of the iron group plotted against metallicity using the same colours for each identified group. Right panels (from top to bottom: i): (i) cumulative age distribution for each group; (ii) mean azimuthal velocity (left *y*-axis and square symbol) and mean dispersion in azimuthal velocity (right *y*-axis and star symbol) for each group as a function of age; (iii) mean vertical velocity (left *y*-axis and square symbol) and mean dispersion in vertical velocity (right *y*-axis and star symbol) for each group as a function of age; (iv) mean metallicity (left *y*-axis and square symbol) and mean dispersion in metallicity (right *y*-axis and star symbol) for each group as a function of age. The error bars in the right panels represent the 95% confidence interval of a bootstrap resampling.
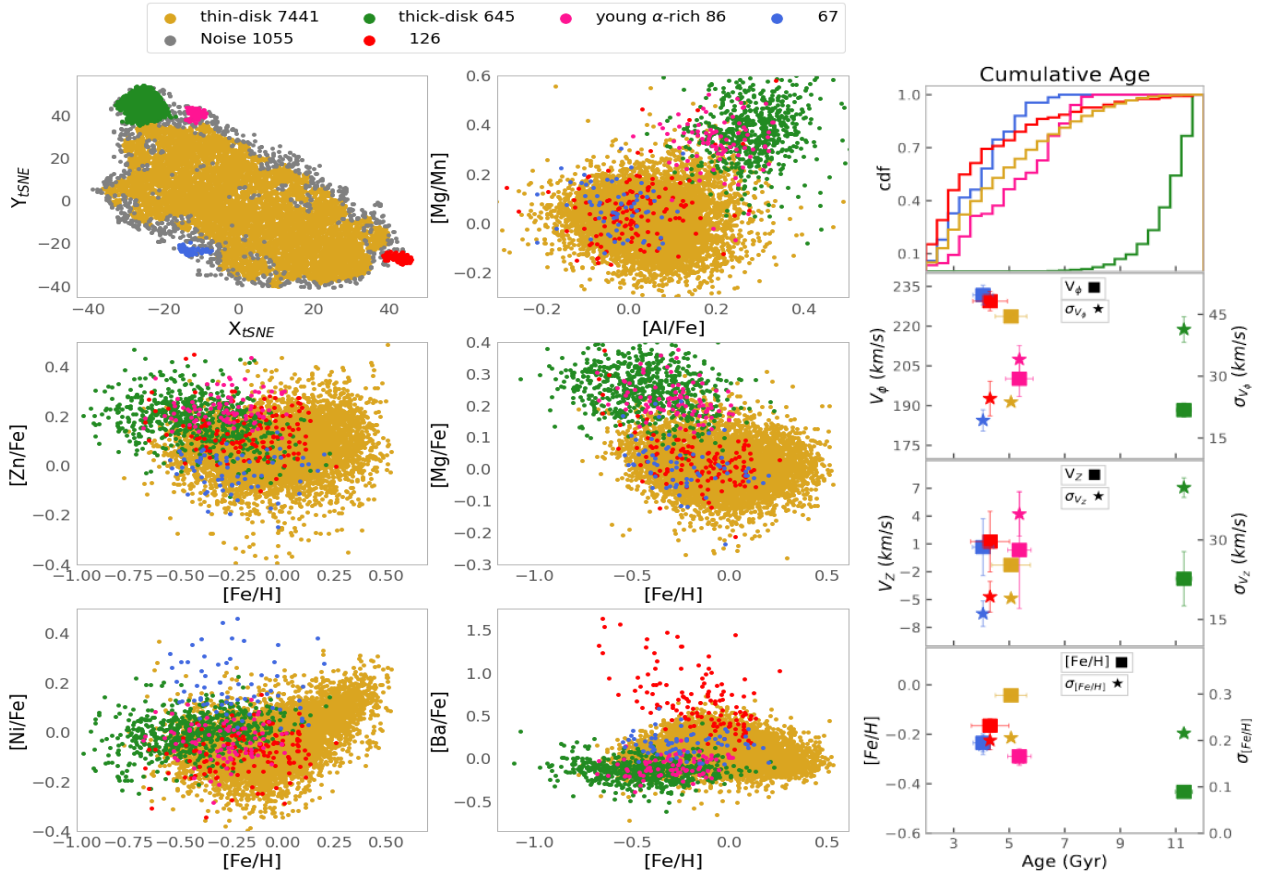
Fig. 5. t-SNE projection for SGB stars in GALAH DR3. Colours correspond to each group found by t-SNE+HDBSCAN from GALAH data. Abundance ratios are also shown, with the same colour coding. Upper panels: cumulative age distribution for each group. Middle panels: mean azimuthal velocity (left axis squares) and mean dispersion in azimuthal velocity (right axis stars) for each group. Lower panels: mean vertical velocity (left axis squares) and mean dispersion in vertical velocity (right axis stars) for each group. The error bars in the right panels represent the 95% confidence interval of a bootstrap resampling.
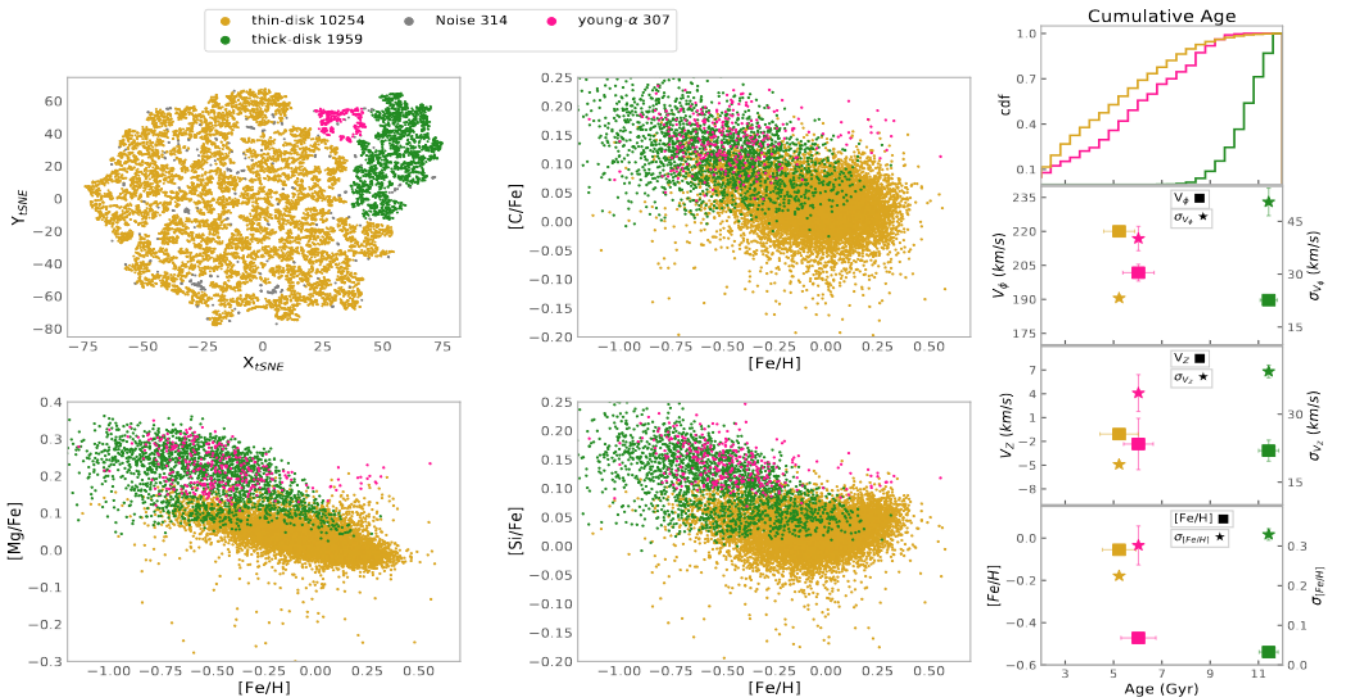

Fig. 6. t-SNE projection for SGB stars in LAMOST MRS. Same as Fig. 4 but for LAMOST MRS data.
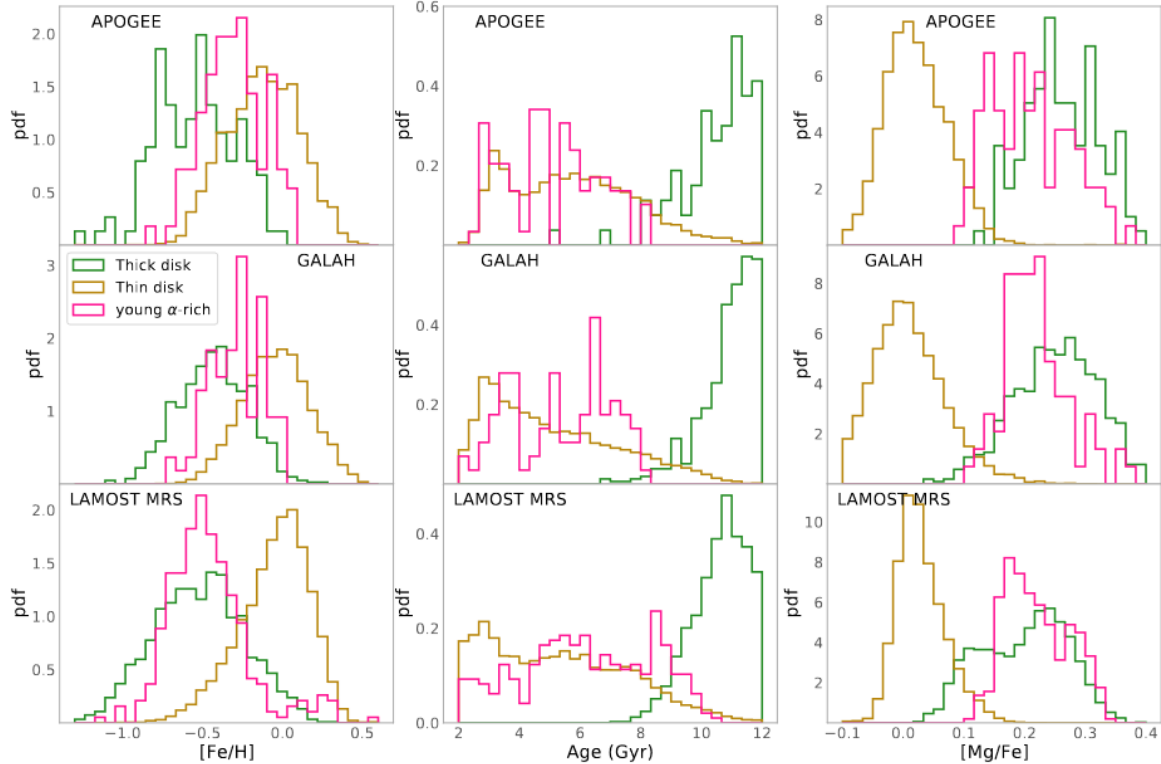
Fig. 7. Probability density function of metallicity, age, and [Mg/Fe] for the main populations found in APOGEE, GALAH, and LAMOST with t-SNE HDBSCAN.

For APOGEE DR17, We obtained a similar grouping configuration, as shown in Fig. 4. No adjustments to the t-SNE and HDBSCAN hyperparameters were necessary, confirming the method's stability on the high-quality APOGEE data. The numbers of young α-rich stars, genuine thick disk stars, and chemical thin disk stars remained roughly unchanged.

For GALAH DR3, We had to modify the random initialisation of the t-SNE hyperparameter, while the HDBSCAN configuration remained unchanged. We successfully recovered the five main groups that passed the robustness tests conducted in Q23. The group member counts remained almost unchanged. However, with the corrected ages, the two small groups (cyan and purple in our original analysis) are not recovered. As discussed in our original work, they were deemed less robust. This is now confirmed this to be the case.

For LAMOST MRS DR7, we adjusted both the perplexity value and its random state. Despite the changes, we retrieved the same three groupings: young α-rich stars, genuine thick disk stars, and thin disk stars. The genuine thick disk group now has more contamination from low-α sequence stars due to the smoother age transition between young and old populations and the lack of more detailed and precise chemistry that would allow a better identification of the different populations.

The age, metallicity, and magnesium distributions for young α-rich and thin disk stars remained roughly unchanged. The distribution of genuine thick disk stars now exhibits a more reasonable age distribution, without the cutoff artefact at around 10 Gyr.

The mean age of the genuine thick disk population is slightly older in all surveys, as observed in Figs. 4–6 and Table 4. The azimuthal velocity and its dispersion were also more consistent with a thick disk population (as before, the genuine thick disks

Table 4. Mean parameters of the genuine thick disk found in the different surveys.

Survey	Age (Gyr)	σ_{age} (Gyr)	V_ϕ (km s^{-1})	σ_{V_ϕ} (km s^{-1})
LAMOST DR7 MRS	11.42	1.34	189.64	50.50
GALAH DR3	11.29	1.06	188.32	41.33
APOGEE DR17	11.20	1.49	179.02	45.65

stars are characterised by a slower rotation and larger velocity dispersion).

5. Impact on the paper conclusions

Our work focusses on providing precise astrophysical parameters for public spectroscopic surveys, along with the inclusion of age estimates for sub-giant and main-sequence turn-off stars. Here we report an error that resulted from a bug in the thin-disc age prior accidentally used in the initial Q23 StarHorse run. All published catalogues have been corrected. The discrepancies with respect to the initial results published in Q23 are relatively minor, and the overall performance of our age estimation method produced good results in both this current run and the previous one.

These catalogues play a critical role in the field of Galactic archaeology, serving as valuable training datasets for machine learning algorithms that can extend and refine these findings to even larger samples. We would like to emphasise that this erratum only addresses the specific issues caused by the incorrect age prior, which include the artificial age cutoff at 10 Gyr and, consequently, the slightly underestimated ages for thick disk stars.

References

Cantat-Gaudin, T., Anders, F., Castro-Ginard, A., et al. 2020, A&A, 640, A1

Kordopatis, G., Schultheis, M., McMillan, P. J., et al. 2023, A&A, 669, A104

Miglio, A., Chiappini, C., Mackereth, J. T., et al. 2021, A&A, 645, A85

Mor, R., Robin, A. C., Figueras, F., & Antoja, T. 2018, A&A, 620, A79

Queiroz, A. B. A., Anders, F., Santiago, B. X., et al. 2018, MNRAS, 476, 2556

Queiroz, A. B. A., Anders, F., Chiappini, C., et al. 2020, A&A, 638, A76

Queiroz, A. B. A., Anders, F., Chiappini, C., et al. 2023, A&A, 673, A155